

**Chiral magnetic effect in the Polyakov–Nambu–Jona-Lasinio model**

Kenji Fukushima\* and Marco Ruggieri†

*Yukawa Institute for Theoretical Physics, Kyoto University, Kyoto 606-8502, Japan*

Raoul Gatto‡

*Departement de Physique Theorique, Universite de Geneve, CH-1211 Geneve 4, Switzerland*

(Received 4 March 2010; published 21 June 2010)

We study the two-flavor Nambu–Jona-Lasinio model with the Polyakov loop in the presence of a strong magnetic field and a chiral chemical potential  $\mu_5$ , which mimics the effect of imbalanced chirality due to QCD instanton and/or sphaleron transitions. First, we focus on the properties of chiral symmetry breaking and deconfinement crossover under the strong magnetic field. Then we discuss the role of  $\mu_5$  on the phase structure. Finally, the chirality charge, electric current, and their susceptibility, which are relevant to the chiral magnetic effect, are computed in the model.

DOI: 10.1103/PhysRevD.81.114031

PACS numbers: 12.38.Aw, 12.38.Mh

**I. INTRODUCTION**

Quantum chromodynamics (QCD) is widely believed to be the theory of the strong interactions. Investigations on its rich vacuum structure and how the QCD vacuum can be modified in an extreme environment are among the major theoretical challenges in modern physics. It is, in particular, an interesting topic to study how nonperturbative features of QCD are affected by thermal excitations at high temperature  $T$  and/or by baryon-rich constituents at large baryon (quark) chemical potential  $\mu_q$ . Such research on hot and dense QCD is important not only from the theoretical point of view but also for numerous applications to the physics problems of the quark-gluon plasma (copiously produced in relativistic heavy-ion collisions), ultradense and cold nuclear/quark matter as could exist in the interior of compact stellar objects, and so on.

The most intriguing nonperturbative aspects of the QCD vacuum at low energy are color confinement and spontaneous breakdown of chiral symmetry. In recent years our knowledge of (some parts of) the QCD phase diagram has increased noticeably because of significant developments of the lattice-QCD simulations (see [1–4] for several examples and see also references therein). At zero  $\mu_q$ , except for some reports [2], the numerical simulations have almost established that two QCD phase transitions (crossovers) take place simultaneously at nearly the same temperature: one for quark deconfinement and another for restoration of chiral symmetry (the latter being always broken because of finite bare quark masses, strictly speaking). It is still under debate whether two crossovers should occur at exactly the same temperature, however.

Once a finite  $\mu_q$  is turned on, the Monte Carlo simulation in three-color QCD on the lattice cannot be performed

straightforwardly because of the (in)famous sign problem [5]. To overcome this problem, several techniques have been developed such as the multiparameter reweighting method [6], Taylor expansion [7], the density of state method [8], analytical continuation from the imaginary chemical potential [9], the complex Langevin dynamics [10], etc.

In addition to hot and dense QCD with  $T$  and  $\mu_q$ , the effect of a strong magnetic field  $\mathbf{B}$  on the QCD vacuum structure is also a very interesting subject. It would be of academic interest to speculate modification of the vacuum structure of a non-Abelian quantum field theory under strong external fields. Besides, more importantly, this kind of investigation has realistic relevance to phenomenology in relativistic heavy-ion collisions in which a strong magnetic field is produced in noncentral collisions [11,12]. In particular, the results obtained by the UrQMD model [12] show that  $eB$  created in noncentral Au-Au collisions can be as large as  $eB \approx 2m_\pi^2$  (i.e.,  $B \sim 10^{18}$  G) for the top collision energy at the Relativistic Heavy Ion Collider, namely,  $\sqrt{s_{NN}} = 200$  GeV. Moreover, an estimate with the energy reachable at LHC,  $\sqrt{s_{NN}} \approx 4.5$  TeV, gives  $eB \approx 15m_\pi^2$  for the Pb-Pb collision according to Ref. [12]. Hence, heavy-ion collisions provide us with a most intriguing laboratory available on the Earth in order to study the effect of extremely strong magnetic fields on the QCD vacuum.

Concerning the (electromagnetic) magnetic field effect on the QCD vacuum structure, there have been many investigations and it has been recognized that  $\mathbf{B}$  plays a role as a catalyzer of dynamical chiral symmetry breaking [13–16]. The QCD vacuum properties have been also studied by means of so-called holographic QCD models [17]. The relation between the dynamics of QCD in a strong magnetic field and noncommutative field theories is investigated in Ref. [18].

A phenomenologically interesting consequence from the strong  $\mathbf{B}$  in heavy-ion collisions is what is termed the chiral

\*fuku@yukawa.kyoto-u.ac.jp

†ruggieri@yukawa.kyoto-u.ac.jp

‡raoul.gatto@unige.ch

magnetic effect (CME) [11,19]. The underlying physics of the CME is the axial anomaly and topological objects in QCD. Analytical and numerical investigations have demonstrated that the sphaleron transition occurs at a copious rate at high temperature unlike instantons that are thermally suppressed [20,21]. Sphalerons are finite-energy solutions of the Minkowskian equations of motion in the pure gauge sector, and they appear not only in the electroweak theory but also in QCD [22]. They carry a finite winding number  $Q_W$ , which is defined as

$$Q_W = \frac{g^2}{32\pi^2} \int d^4x \text{Tr}[F\tilde{F}], \quad (1)$$

where  $F$  and  $\tilde{F}$  denote, respectively, the field strength tensor and its dual. Sphalerons connect two distinct classical vacua of the theory with different Chern-Simons numbers in Minkowskian space-time. It is possible through the coupling with fermions in the theory to relate the change of chirality  $N_R - N_L$  to the winding number by virtue of the Adler-Bell-Jackiw anomaly relation

$$(N_R - N_L)_{t=+\infty} - (N_R - N_L)_{t=-\infty} = -2Q_W. \quad (2)$$

The right-hand side of Eq. (2) is the integral over space-time of  $\partial_\mu j_5^\mu$ , where  $j_5^\mu$  represents the anomalous flavor-singlet axial current. The physical picture that arises from Eq. (2) is that in the presence of topological excitations such as instantons and sphalerons with a given  $Q_W$ , and starting with a system of quarks with  $N_R = N_L$ , an imbalance between left-handed and right-handed quarks is produced. Such an imbalance can lead to observable effects to probe topological  $\mathcal{P}$ - and  $\mathcal{CP}$ -odd excitations. An experimental observable sensitive to local  $\mathcal{P}$ - and  $\mathcal{CP}$ -odd effects has been proposed in Ref. [23]. Recently, the STAR Collaboration presented the conclusive observation of charge azimuthal correlations [24] possibly resulting from the CME with local  $\mathcal{P}$  and  $\mathcal{CP}$  violation.

The intuitive picture of the CME is as follows. In a strong magnetic field  $\mathbf{B}$ , quarks are polarized along the direction of  $\mathbf{B}$ . Let us suppose that  $\mathbf{B}$  is along the positive  $z$  axis (that is conventionally taken as the  $y$  axis in the context of heavy-ion collisions). By neglecting quark masses, which is a good approximation for  $u$  and  $d$  quarks in the high- $T$  chiral restored phase, the chirality is an eigenvalue to label the quarks. Then, right-handed  $u$  quarks should have both their spin and momentum parallel to  $\mathbf{B}$ , and left-handed  $u$  quarks should have their spin parallel to  $\mathbf{B}$  and momentum antiparallel to  $\mathbf{B}$ . Obviously, the same reasoning applies to  $d$  quarks. If  $N_R = N_L$ , then the current that would originate from the motion of left-handed quarks is exactly canceled by that of right-handed quarks. If  $N_R \neq N_L$ , which is expected from the anomaly relation (2), on the other hand, a finite net current is produced. Therefore, if quarks experience a strong magnetic field in a domain where the topological transition occurs, a net current is produced locally.

The CME has been investigated in the chiral effective model [25] as well as in the holographic QCD model [17]. The chiral magnetic conductivity is calculated without gluon interactions in Ref. [26]. In Ref. [27], the electric-current susceptibility under a homogeneous magnetic field, which can be related to the fluctuation of the electric-charge asymmetry measured by the STAR Collaboration, has been computed in the same way. The first lattice-QCD study of the CME has been performed by the Institute for Theoretical and Experimental Physics lattice group [28] in the color-SU(2) quench approximation. Moreover, the Connecticut group [29] performed a lattice-QCD study of the CME with 2 + 1 dynamical quark flavors.

This paper is devoted to the study of the two-flavor Nambu–Jona-Lasinio model with the Polyakov loop coupling (PNJL model) in a strong magnetic field. The PNJL model has been introduced in Refs. [30,31] to incorporate deconfinement physics into the NJL model [32]. The main addition to the NJL model is a background gluon field in the Euclidean temporal direction. The background field is related to the expectation value of the traced Polyakov loop  $\Phi$ , which is known to be an order parameter for the deconfinement transition in a pure gauge theory [33]. There are many theoretical studies related to different aspects of the PNJL model; see, for example, Ref. [34]. See Ref. [35] for a related study within the Polyakov-quark-meson model and Ref. [36] for an investigation within QCD with imaginary chemical potential.

We work in the chiral limit throughout the paper, in which the definition of the chiral critical temperature has no ambiguity. First, we focus on the effect of  $\mathbf{B}$  on chiral symmetry restoration at finite temperature. As will be clear soon, our results support the role of the external  $\mathbf{B}$  as a catalyzer of dynamical symmetry breaking; the critical temperature increases with increasing  $\mathbf{B}$ . Naturally, the (pseudo)critical temperature for deconfinement crossover is less sensitive to the presence of  $\mathbf{B}$  because there is no direct coupling between photons and gluons. Hence, the PNJL model predicts that at large enough  $\mathbf{B}$ , a substantial range of temperature will open at which quark matter is deconfined but chiral symmetry is still dynamically broken. See [37] for a related study.

Also we shall discuss the effects of a finite chiral chemical potential  $\mu_5$  on the phase structure within the PNJL model. This  $\mu_5$  mimics the topologically induced changes in chirality charges  $N_5 = N_R - N_L$  that are naturally expected by the QCD anomaly relation. The relevant quantity in a microscopic picture is rather the total chirality charge  $N_5$ , but for technical reasons it is easier to work in the grand-canonical ensemble by treating  $\mu_5$  (see Ref. [38] for an alternative description based on the flux-tube picture), which is to be interpreted as the time derivative of the  $\theta$  angle of the strong interactions;  $\mu_5 = \dot{\theta}/(2N_f)$ . Besides the phase diagram from the PNJL model, we compute quantities that are relevant to the CME, namely, the in-

duced electric-current density, its susceptibility, and the chiral charge density  $n_5$  together with its susceptibility.

This paper is organized as follows; in Sec. II, we give a detailed description of the model we are using. In Secs. III and IV, we present and discuss our numerical results from the model. Finally, in Sec. V, we draw our conclusions.

## II. MODEL WITH MAGNETIC FIELD AND CHIRAL CHEMICAL POTENTIAL

In this section we analyze the interplay between the chiral phase transition and the deconfinement crossover at large  $\mathbf{B}$  by using the PNJL model. Here we consider two-flavor quark matter in the chiral limit since the chiral phase transition is a true phase transition only in the chiral limit, and then and only then  $T_c$  can be identified unambiguously by a vanishing chiral condensate. The chiral limit in the two-flavor sector is not far from the physical world in which the current quark masses are a few MeV, almost negligible as compared to the temperature. Moreover, we are interested in studying the situation in the presence of chirality-charge density. In the grand-canonical ensemble we can introduce the chirality charge by virtue of the associated chemical potential  $\mu_5$  in the following way.

The Lagrangian density of the model we consider is given by

$$\mathcal{L} = \bar{\psi}(i\gamma_\mu D^\mu + \mu_5\gamma^0\gamma^5)\psi + G[(\bar{\psi}\psi)^2 + (\bar{\psi}i\gamma^5\boldsymbol{\tau}\psi)^2] - \mathcal{U}[\Phi, \bar{\Phi}, T], \quad (3)$$

where the covariant derivative embeds the quark coupling to the external magnetic field and to the background gluon field as well, as we will see explicitly below. We note that  $\mu_5$  couples to the chiral density operator  $\mathcal{N}_5 = \bar{\psi}\gamma^0\gamma^5\psi = \psi_R^\dagger\psi_R - \psi_L^\dagger\psi_L$ ; hence  $n_5 = \langle\mathcal{N}_5\rangle \neq 0$  can develop when  $\mu_5 \neq 0$ . The mean-field Lagrangian is then given by

$$\mathcal{L} = \bar{\psi}(i\gamma_\mu D^\mu - M + \mu_5\gamma^0\gamma^5)\psi - \mathcal{U}[\Phi, \bar{\Phi}, T], \quad (4)$$

where  $M = -2\sigma$  with  $\sigma = G\langle\bar{\psi}\psi\rangle = G(\langle\bar{u}u\rangle + \langle\bar{d}d\rangle)$ .

In Eq. (4),  $\Phi$  and  $\bar{\Phi}$  correspond to the normalized traced Polyakov loop and its Hermitian conjugate, respectively,  $\Phi = (1/N_c)\text{Tr}L$  and  $\bar{\Phi} = (1/N_c)\text{Tr}L^\dagger$ , with the Polyakov loop matrix

$$L = \mathcal{P}\exp\left(i\int_0^\beta A_4 d\tau\right), \quad (5)$$

where  $\beta = 1/T$ .

The potential term  $\mathcal{U}[\Phi, \bar{\Phi}, T]$  in Eq. (4) is built by hand in order to reproduce the pure gluonic lattice data [34]. Among several different potential choices [39] we adopt the following logarithmic form [31,34]:

$$\mathcal{U}[\Phi, \bar{\Phi}, T] = T^4\left\{-\frac{a(T)}{2}\bar{\Phi}\Phi + b(T)\ln[1 - 6\bar{\Phi}\Phi] + 4(\bar{\Phi}^3 + \Phi^3) - 3(\bar{\Phi}\Phi)^2\right\}, \quad (6)$$

with three model parameters (one of four is constrained by the Stefan-Boltzmann limit)

$$a(T) = a_0 + a_1\left(\frac{T_0}{T}\right) + a_2\left(\frac{T_0}{T}\right)^2, \quad b(T) = b_3\left(\frac{T_0}{T}\right)^3. \quad (7)$$

The standard choice of the parameters reads [34]

$$\begin{aligned} a_0 &= 3.51, & a_1 &= -2.47, \\ a_2 &= 15.2, & b_3 &= -1.75. \end{aligned} \quad (8)$$

The parameter  $T_0$  in Eq. (6) sets the deconfinement scale in the pure gauge theory, i.e.,  $T_c = 270$  MeV.

We assume a homogeneous magnetic field  $\mathbf{B}$  along the positive  $z$  axis. The eigenvalues of the Dirac operator can be derived by the Ritus method [40] and are [19]

$$\omega_s^2 = M^2 + [|\mathbf{p}| + s\mu_5\text{sgn}(p_z)]^2, \quad (9)$$

apart from (the phases of) the Polyakov loop, where  $s = \pm 1$ ,  $\mathbf{p}^2 = p_z^2 + 2|q_f B|k$ , with  $k$  a non-negative integer labeling the Landau level.

The thermodynamical potential  $\Omega$  in the mean-field approximation in the presence of an Abelian chromomagnetic field has been considered in much of the literature, Ref. [41], for example. The expression for an electromagnetic  $\mathbf{B}$  can be obtained in the same way. Here we simply write the final result:

$$\begin{aligned} \Omega &= \mathcal{U} + \frac{\sigma^2}{G} - N_c \sum_{f=u,d} \frac{|q_f B|}{2\pi} \sum_{s,k} \alpha_{sk} \int_{-\infty}^{\infty} \frac{dp_z}{2\pi} f_\Lambda^2 \omega_s(p) \\ &\quad - 2T \sum_{f=u,d} \frac{|q_f B|}{2\pi} \sum_{s,k} \alpha_{sk} \int_{-\infty}^{\infty} \frac{dp_z}{2\pi} \\ &\quad \times \ln(1 + 3\Phi e^{-\beta\omega_s} + 3\bar{\Phi} e^{-2\beta\omega_s} + e^{-3\beta\omega_s}). \end{aligned} \quad (10)$$

Here the above definition of  $\Omega$  is different from the standard grand potential in thermodynamics by a volume factor  $V$ . The quasiparticle dispersion  $\omega_s$  is given by Eq. (9). The spin degeneracy factor is

$$\alpha_{sk} = \begin{cases} \delta_{s,+1} & \text{for } k = 0, qB > 0, \\ \delta_{s,-1} & \text{for } k = 0, qB < 0, \\ 1 & \text{for } k \neq 0. \end{cases} \quad (11)$$

Before going ahead further, one may wonder why we introduce only one order parameter for the chiral symmetry breaking even though the magnetic field breaks isospin symmetry. Since  $q_u \neq q_d$ , one could suspect that the effects of  $\mathbf{B}$  on  $\langle\bar{u}u\rangle$  and on  $\langle\bar{d}d\rangle$  are different. This is not the case, however, in the present model in the mean-field

approximation. As a matter of fact, even in the presence of  $\mathbf{B} \neq 0$ , the thermodynamic potential (10) depends only on  $\sigma \propto \langle \bar{u}u \rangle + \langle \bar{d}d \rangle$ . This is so only when the four-fermion interaction is Eq. (3) with equal mixing of the  $U(1)_A$ -symmetric and  $U(1)_A$ -breaking terms. Hence, the relevant quantity for the chiral symmetry breaking is just one condensate, namely,  $\sigma$ , even for  $\mathbf{B} \neq 0$ , and there is no need to introduce two independent condensates in this special case. Even when we consider more general four-fermion interaction, the isospin breaking effect is only negligibly small.

The vacuum part of the thermodynamic potential,  $\Omega(T=0)$ , is ultraviolet divergent. This divergence is transmitted to the gap equations. Thus we must specify a scheme to regularize this divergence. The choice of the regularization scheme is a part of the model definition, but, nevertheless, the physically meaningful results should not depend on the regulator eventually. In the case with a strong magnetic field the sharp momentum cutoff suffers from a cutoff artifact since the continuum momentum is replaced by the discrete Landau quantized one. To avoid a cutoff artifact, in this work, we use a smooth regularization procedure by introducing a form factor  $f_\Lambda(p)$  in the diverging zero-point energy. Our choice of  $f_\Lambda(p)$  is as follows:

$$f_\Lambda(p) = \sqrt{\frac{\Lambda^{2N}}{\Lambda^{2N} + |\mathbf{p}|^{2N}}}, \quad (12)$$

where we specifically choose  $N = 10$ . In the  $N \rightarrow \infty$  limit, the above  $f_\Lambda(p)$  is reduced to the sharp cutoff function  $\theta(\Lambda - |\mathbf{p}|)$ . Since the thermal part of  $\Omega$  is not divergent, we do not need to introduce a regularization function.

### III. PHASE STRUCTURE WITH CHIRAL CHEMICAL POTENTIAL

In this section we first focus on the system at  $\mu_5 = 0$  and discuss the role of the magnetic field as a catalyzer of the dynamical chiral symmetry breaking. We also analyze the interplay between chiral symmetry restoration and deconfinement crossover as the strength of  $\mathbf{B}$  increases.

#### A. Results at $\mu_5 = 0$ —chiral symmetry breaking and deconfinement

We analyze, within the PNJL model, the response of quark matter to  $\mathbf{B}$  at  $\mu_5 = 0$ . In particular, we are interested in the interplay between chiral symmetry restoration and deconfinement crossover in the presence of a magnetic field, which leads to the so-called chiral magnetic catalysis [14]. Our model parameter set is

$$\Lambda = 620 \text{ MeV}, \quad G\Lambda^2 = 2.2. \quad (13)$$

These parameters correspond to  $f_\pi = 92.4 \text{ MeV}$  and the vacuum chiral condensate  $\langle \bar{u}u \rangle^{1/3} = -245.7 \text{ MeV}$ , and

the constituent quark mass  $M = 339 \text{ MeV}$ . The critical temperature for chiral restoration in the NJL part at  $\mathbf{B} = 0$  is  $T_c \approx 190 \text{ MeV}$ . We set the deconfinement scale  $T_0$  in the Polyakov loop potential [see Eq. (6)] as  $T_0 = 270 \text{ MeV}$ , which is the value of the known deconfinement temperature in the pure SU(3) gauge theory.

In Fig. 1, we plot the absolute value of the chiral condensate  $\langle \bar{u}u \rangle^{1/3}$  (upper panel) and expectation value of the Polyakov loop (lower panel) as a function of  $T$  computed at several values of  $eB$  (expressed in units of  $m_\pi^2$ ). The chiral condensate  $\langle \bar{u}u \rangle$  and the Polyakov loop  $\Phi$  are the solution of the gap equations  $\partial\Omega/\partial\sigma = \partial\Omega/\partial\Phi = 0$  in the model at hand.

Figure 1 is interesting for several reasons. First of all, the role of  $\mathbf{B}$  as a catalyzer of chiral symmetry breaking is evident. Indeed, the chiral condensate and thus constituent quark mass increase in the whole  $T$  region as  $eB$  is raised. (For graphical reasons, we have plotted our results starting from  $T = 100 \text{ MeV}$ . There is nevertheless no significant numerical difference between the  $T = 0$  and  $T = 100 \text{ MeV}$  results.) This behavior is in the correct direction

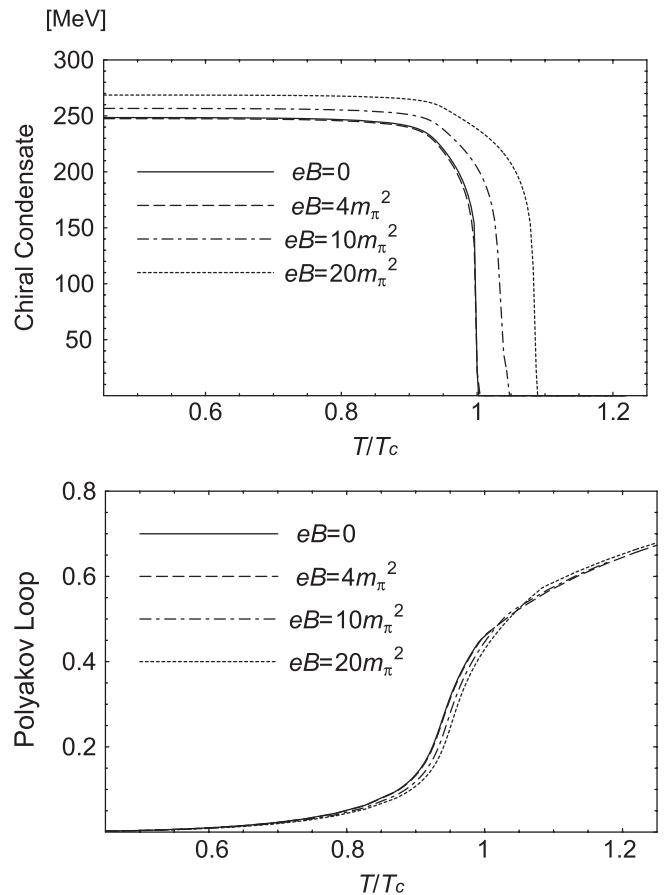


FIG. 1. Absolute value of the chiral condensate  $|\langle \bar{u}u \rangle^{1/3}|$  (upper panel) and expectation value of the Polyakov loop (lower panel) as a function of  $T$  computed at several values of  $eB$  (in units of  $m_\pi^2$ ). In this model  $T_c = 228 \text{ MeV}$  at  $\mu_5 = B = 0$ .

consistent with the well-known magnetic catalysis revealed in Ref. [14] and also discussed recently in Ref. [41] in a slightly different context of the PNJL-model study on the response of quark matter to external chromo-magnetic fields.

Second, we observe that the deconfinement crossover is only marginally affected by the magnetic field. We can identify the deconfinement  $T_c$  by the inflection point of  $\Phi$  as a function of  $T$ . This simple procedure gives results nearly in agreement with those obtained by the peak position in the Polyakov loop susceptibility, which is a common prescription to locate the so-called pseudocritical temperature. Also, we can identify the deconfinement  $T_c$  with the temperature at which  $\Phi = 0.5$ . We note that  $T_c$  in Fig. 1 is the chiral  $T_c = 228$  MeV where the chiral condensate vanishes, but not the deconfinement  $T_c$  in both figures.

From Fig. 1 we notice that, by increasing  $eB$  from  $4m_\pi^2$  to  $20m_\pi^2$ , the shift of the chiral transition temperature  $\Delta T_\chi \approx 20$  MeV, while the shift of the deconfinement crossover temperature is as small as  $\Delta T_\Phi \approx 5$  MeV. Hence, the chiral phase transition is more easily influenced by the magnetic field than the deconfinement as anticipated. Consequently, under a strong magnetic field, there opens a substantially wide  $T$  window in which quarks are deconfined but chiral symmetry is still spontaneously broken. This result, valid for  $\mu_5 = 0$ , does not necessarily hold, in general, for  $\mu_5 \neq 0$ , as we will see in the next subsection.

### B. Results at $\mu_5 \neq 0$ —suppression on the chiral condensate

We next turn to the study of the effect of a finite  $\mu_5$  on the QCD phase transitions using the PNJL model. We recall that  $\mu_5$  cannot be a true chemical potential since its conjugate variable  $n_5$  is only approximately conserved due to axial anomaly. Nevertheless, because the time derivative of the strong  $\theta$  angle translates into  $\mu_5$ , as explained in the introduction,  $\mu_5$  itself is a physically meaningful quantity. We specifically look into the behavior of the critical line for chiral symmetry restoration, which is well defined in the chiral limit, at differing  $B$  while keeping  $\mu_5$  fixed. This study will be useful, among other things, in order to understand the relation between the chirality density  $n_5$  and  $\mu_5$  that we compute numerically in later discussions.

One effect of  $\mu_5 \neq 0$  is lowering of the critical temperature of the chiral phase transition. This is evident from the upper panels of Fig. 2. First, we discuss the case of  $eB = 5m_\pi^2$  corresponding to the left upper and left lower panels of Fig. 2. We see that increasing  $\mu_5$  at low  $T$  results in slight enhancement of the chiral condensate. As  $T$  approaches  $T_c$ , however, the chiral phase transition at larger  $\mu_5$  takes place earlier below  $T_c$ . As a result of the coupling between the chiral condensate and the Polyakov loop, the

deconfinement crossover as shown in the lower panels of Fig. 2 is also shifted earlier as  $\mu_5$  becomes greater.

In view of the right upper and right lower panels of Fig. 2 for large  $eB = 10m_\pi^2$  the  $\mu_5$  effect on the chiral condensate at low  $T$  is less visible. This is understood from the fact that the chiral magnetic catalysis effect is predominant over the minor enhancement due to  $\mu_5$ . In contrast, as  $T$  is increased toward  $T_c$ , the qualitative behavior of the shift in the critical temperature is just the same as what we have seen previously for  $eB = 5m_\pi^2$ .

An interesting prediction from the PNJL model is that, at a given value of  $eB$ , there exists a critical  $\mu_5$ , above which the chiral phase transition becomes first-order. In the case  $eB = 5m_\pi^2$  as shown in Fig. 2, the critical  $\mu_5$  is found between 300 and 400 MeV. As a matter of fact, at  $\mu_5 = 400$  MeV, the chiral condensate and the Polyakov loop both exhibit discontinuity at the critical temperature. We see that, as compared to the  $\mu_5 = 300$  MeV case, the slopes of the chiral condensate and the Polyakov loop sharply change as a function of  $T$  for the  $\mu_5 = 400$  MeV case. Hence, our data plotted in Fig. 2 suggest the existence of a critical  $\mu_5$  in the range  $300 \text{ MeV} < \mu_5^c < 400 \text{ MeV}$  at which the weakly first-order transition becomes a true second-order one. The phase diagram in the  $\mu_5$ - $T$  plane has a tricritical point (TCP) accordingly. We will discuss more on the TCP in the next subsection. We notice that this picture is qualitatively robust regardless of the chosen value of  $eB$ , as is already implied from Fig. 2. The first-order phase transition in the high- $\mu_5$  and low- $T$  region leads to a discontinuity in the chirality density as a function of  $\mu_5$ . This point will also be addressed in some detail in the next section.

As a final remark in this subsection we note that, in Figs. 1 and 2, the slope of the curve quickly changes at some point (at  $T/T_c = 1$  for  $eB = 0$ , for example). This is because of the second-order phase transition, which is the case for chiral restoration in the chiral limit.

### C. Phase diagram

The results we have revealed so far can be summarized into the phase diagram in the  $\mu_5$ - $T$  plane. In the upper panel of Fig. 3, we show the phase diagram at  $eB = 5m_\pi^2$ . In the lower panel, for comparison we plot the phase diagram at  $eB = 15m_\pi^2$ . The line represents the chiral phase transition. It is of second order for small values of  $\mu_5$  (shown by a thin line) and becomes of first order at large  $\mu_5$  (shown by a thick line). The location of the TCP on the phase diagram depends only slightly on  $eB$ , while the topology of the phase diagram is not sensitive to the magnetic field.

The general effect of  $\mu_5$  is to lower the chiral transition temperature. One may argue that the critical line can hit  $T = 0$  eventually at very large  $\mu_5$ , though the PNJL model is of no use at such large  $\mu_5$  because the ultraviolet cutoff causes unphysical artifacts. The locations of the TCP are

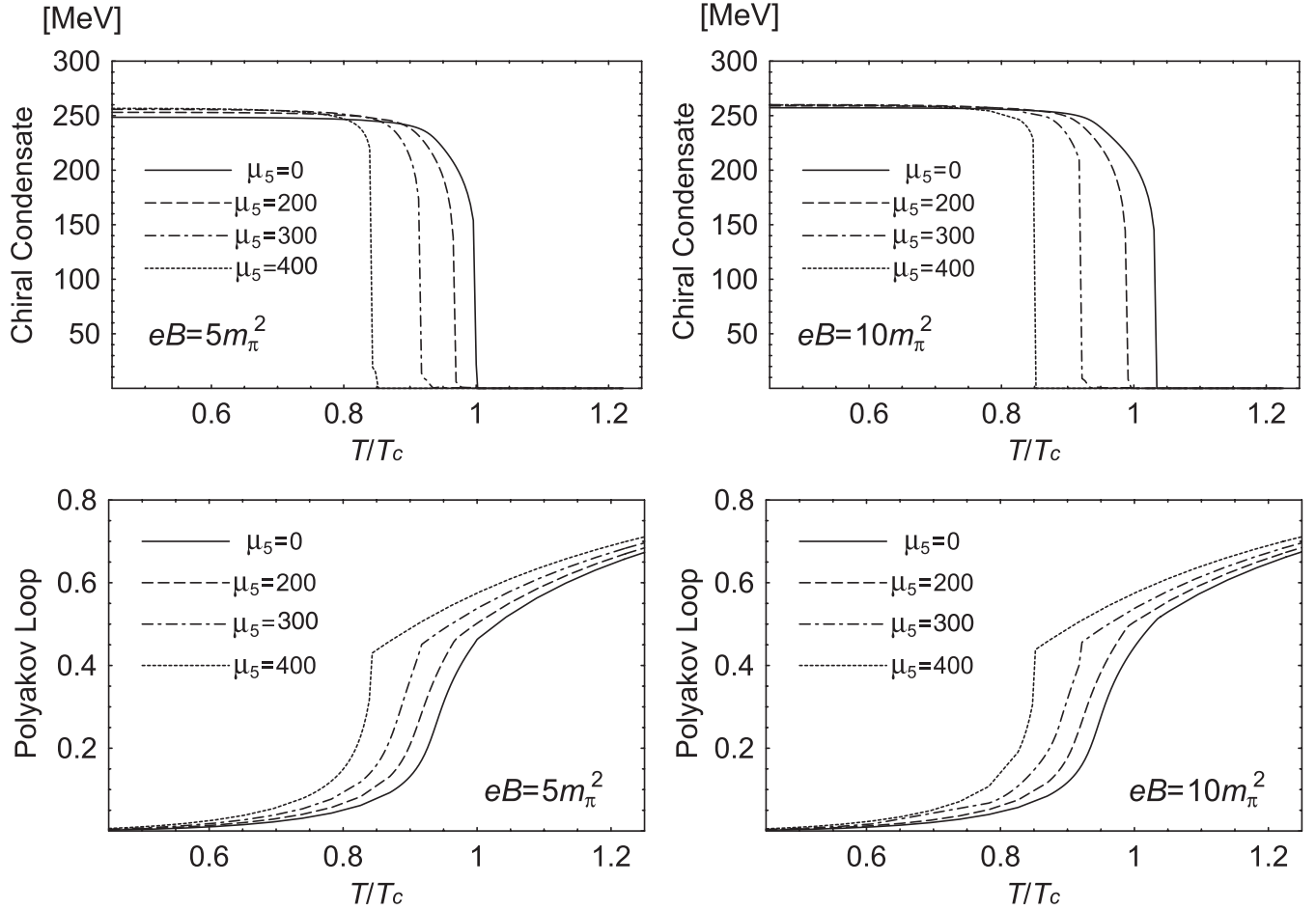


FIG. 2. Absolute value of the chiral condensate  $|\langle \bar{u}u \rangle|^{1/3}$  (upper panel) and expectation value of the Polyakov loop (lower panel) as a function of  $T$  computed at several values of  $eB$  (in units of  $m_\pi^2$ ) and  $\mu_5$  (in units of MeV).

estimated from the PNJL model as

$$(\mu_5, T) \approx (400 \text{ MeV}, 200 \text{ MeV}), \quad \text{for } eB = 5m_\pi^2, \quad (14)$$

$$(\mu_5, T) \approx (370 \text{ MeV}, 200 \text{ MeV}), \quad \text{for } eB = 15m_\pi^2. \quad (15)$$

#### IV. CHIRALITY CHARGE, ELECTRIC CURRENT, AND SUSCEPTIBILITIES

In this section we show our results for quantities relevant to the CME. We numerically compute the chiral density  $n_5$  and its susceptibility  $\chi_5$  as a function of  $\mu_5$  and  $eB$ . Also we calculate the current density  $j_3$  along the direction of  $\mathbf{B}$  and its susceptibility  $\chi_J$ . Finally, we use the result  $n_5(\mu_5)$  to evaluate  $j_3$  as a function of  $n_5$ .

##### A. Chirality density and its susceptibility

The axial anomaly relates the topological charge  $Q_W$  to the chirality charge  $N_5$ , with  $N_5 = n_5 V$ , where  $V = L_x L_y L_z$  is the volume of topological domains. We can

read  $n_5$  from

$$n_5 = -\frac{\partial \Omega}{\partial \mu_5}. \quad (16)$$

It is useful information to relate  $n_5$  and  $\mu_5$  for various temperatures and magnetic field strengths. In the next section we will use the results of  $n_5(\mu_5)$  to express the current density as a function of the chirality density.

The relation between  $n_5$  and  $\mu_5$  can be found analytically only in simple limiting cases [19]. In general, one has to determine it numerically by using an effective model. We show  $n_5(\mu_5)$  for  $eB = 5m_\pi^2$  at three temperatures around  $T_c$  in Fig. 4. The qualitative picture is hardly modified even if we change the magnetic field.

From Fig. 3 we can read the critical temperature at  $\mu_5 = 0$  that is  $T_c = 228$  MeV. At temperatures well below  $T_c$ , as seen in the  $T = 160$  MeV case in Fig. 4, the discontinuity associated with the first-order phase transition with respect to  $\langle \bar{u}u \rangle|^{1/3}$  and  $\Phi$  is conveyed to the relation  $n_5(\mu_5)$ , which is a typical manifestation of the mixed phase at critical  $\mu_5$ . Naturally, as  $T$  gets larger, the chirality density as a func-

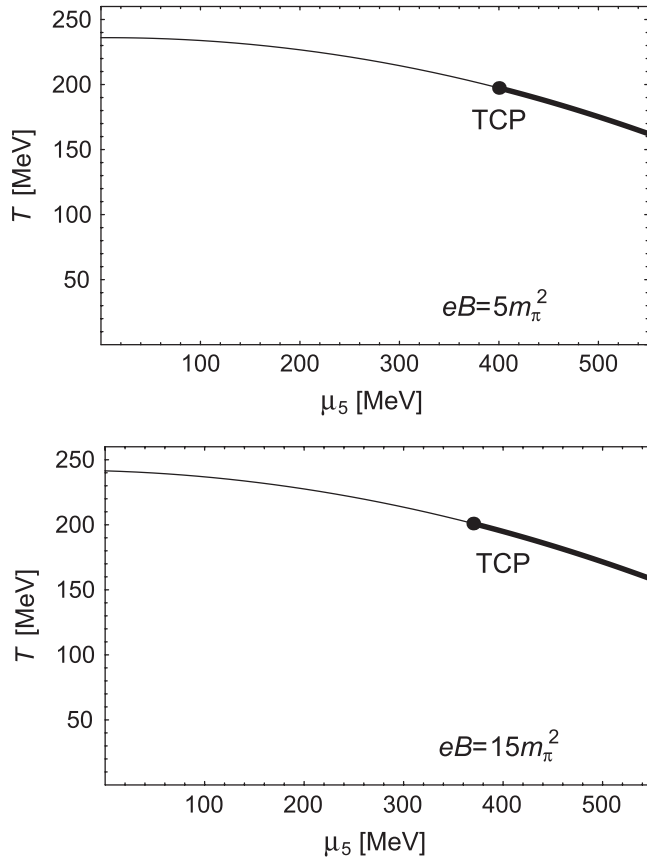


FIG. 3. (Upper panel) Phase diagram in the  $\mu_5$ - $T$  plane obtained at  $eB = 5m_\pi^2$ . The thin line represents a second-order chiral phase transition and the thick one a first-order transition. Below the line, chiral symmetry is spontaneously broken, while chiral symmetry is restored above the line. The label “TCP” denotes the tricritical point. (Lower panel) Phase diagram for  $eB = 15m_\pi^2$ .

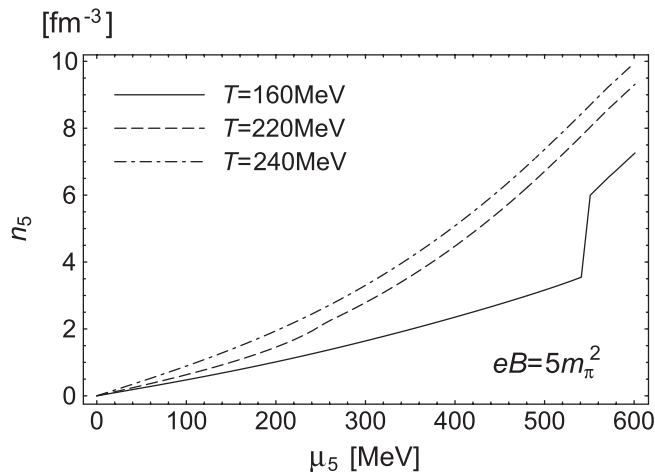


FIG. 4. Chirality density  $n_5$  (in units of  $\text{fm}^{-3}$ ) as a function of  $\mu_5$  (in units of MeV) at  $eB = 5m_\pi^2$  for several values of  $T$ .

tion of  $\mu_5$  becomes smoother, since the chiral phase transition is of second order at higher  $T$  as is clear from Fig. 3.

It is interesting to compute the chirality-charge susceptibility  $\chi_5$ , as well as  $n_5$ , defined as

$$\chi_5 = \langle n_5^2 \rangle - \langle n_5 \rangle^2 = -\frac{1}{\beta V} \frac{\partial^2 \Omega}{\partial \mu_5^2}, \quad (17)$$

where  $\beta = 1/T$  and  $V$  is the volume. We note that this definition of the susceptibility is different from that in Ref. [27] by  $V$ . It should be mentioned that we take a numerical derivative to compute  $\chi_5$  including implicit dependence in  $\Phi$  and  $\sigma$ . In Fig. 5, we plot  $\chi_5$  as a function of  $eB$  for several  $\mu_5$  values. The upper panel corresponds to  $\mu_5 = 0$ , the middle one to  $\mu_5 = 200$  MeV, and the lower one to  $\mu_5 = 400$  MeV. For completeness, in the right panels of the same Fig. 5, we plot the chiral condensate  $|\langle \bar{u}u \rangle|^{1/3}$  for the same  $T$  and same  $\mu_5$ . The oscillations in  $\chi_5$  are artificial results because of the momentum cutoff  $\Lambda$ . As shown in Ref. [41], by choosing a regulator which is smoother than used in this work, the oscillations of the various quantities could be erased. The qualitative picture is, nevertheless, unchanged even with a different regulator. For this reason we do not perform a systematic study here on the cutoff scheme dependence.

A notable aspect is the suppression of the chirality-charge fluctuations at large  $T$  and large  $eB$ . This is evident, for example, in the result with  $\mu_5 = 0$  and  $T = 1.1T_c$  in Fig. 5. As long as  $eB$  is small,  $\chi_5$  is a monotonously increasing function of  $eB$  as expected naively. When  $eB$  reaches a critical value around  $20m_\pi^2$ , however,  $\chi_5$  has a pronounced peak and then decreases with increasing  $eB$ , which is a result of mixture with diverging chiral susceptibility at the chiral phase transition. It should be mentioned that  $\chi_5$  at  $\mu_5 = 0$  (as shown in the upper left panel of Fig. 5) does not diverge at the critical  $eB$  since the mixing with the chiral susceptibility is vanishing due to  $\mu_5 = 0$ . This behavior below and above the chiral critical point can be easily understood in terms of the chiral symmetry breaking by virtue of the magnetic field. As a matter of fact, at  $T > T_c$  the chiral condensate stays zero identically as long as  $eB$  is small enough, leading to zero quasiparticle masses. Once  $eB$  exceeds a critical value, the chiral symmetry is broken spontaneously even at high  $T$  (see the upper right panel of Fig. 5) and the quasiparticle masses can then jump to a substantially large number. Such dynamical quark masses result in appreciable suppression of the chirality-charge fluctuations. As will be shown in the next section, this interesting and intuitively understandable effect appears in the current susceptibility as well.

## B. Current density and its susceptibility

The current density  $j_3$  (and its susceptibility as well) is the most important quantity to compute for the chiral magnetic effect [27]. It corresponds to the charge per unit volume that moves in the direction of the applied

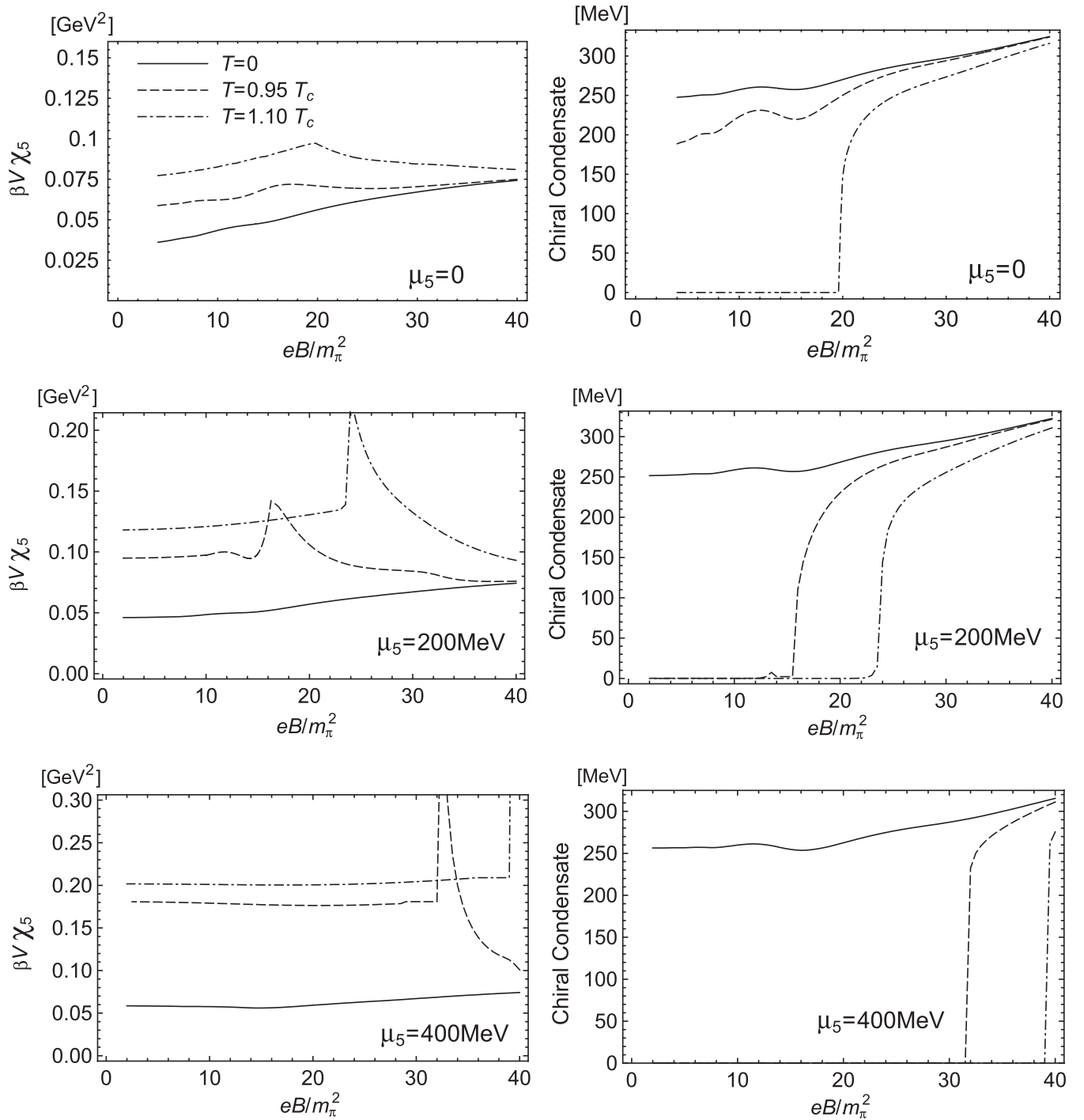


FIG. 5. (Left panels) Chirality-charge susceptibility  $\chi_5$  as a function of  $eB$  (in units of  $m_\pi^2$ ) for several temperatures. The chiral chemical potential is chosen as  $\mu_5 = 0, 200 \text{ MeV}$ , and  $400 \text{ MeV}$ , respectively, from the upper to the lower panels. The solid line corresponds to  $T = 0$ , the dashed line to  $T = 0.95 T_c$ , and the dotted-dashed line to  $T = 1.1 T_c$ . Here  $T_c = 228 \text{ MeV}$  is the critical temperature in this model at  $\mu_5 = B = 0$ . (Right panels) Absolute value of the chiral condensate  $\langle \bar{u}u \rangle^{1/3}$  as a function of  $eB$ . The line styles are the same as defined in the left upper panel.

magnetic field in a domain where an instanton/sphaleron transition takes place, which causes chirality change of quarks. The current has been computed analytically in Ref. [19] in four different ways.

To compute the current density along the magnetic field, i.e.,  $j_3 = q \langle \bar{\psi} \gamma_3 \psi \rangle$ , we follow the common procedure to add an external homogeneous vector potential along the magnetic field,  $A_3$ , coupled to the fermion field. Then

$$j_3 = - \left. \frac{\partial \Omega}{\partial A_3} \right|_{A_3=0}. \quad (18)$$

The derivative of the thermodynamic potential in the presence of a background field is computed in the following way. The coupling of quarks to  $A_3$  is achieved by shifting  $p_z$  in Eq. (10) as  $p_z \rightarrow p_z + q_f A_3$ . After putting regularization in the momentum integral with an ultraviolet cutoff  $\Lambda$  (we know that the current is ultraviolet finite; hence the choice of the regularization method does not affect the final result), we change the order of the momentum integral and the derivative with respect to  $A_3$ . Then we make use of the following replacement:

$$\frac{\partial}{\partial A_3} \rightarrow q_f \frac{d}{dp_z}, \quad (19)$$

to obtain

$$j_3 = N_c \sum_{f=u,d} q_f \frac{|q_f B|}{2\pi} \sum_{s,k} \alpha_{ks} \int_{-\Lambda}^{\Lambda} \frac{dp_z}{2\pi} \frac{d}{dp_z} [\omega_s(p) + \dots]. \quad (20)$$

The ellipsis represents irrelevant matter terms. After summing over the spin  $s$ , the contribution of the integrand from the Landau levels with  $n > 0$  turns out to be an odd function of  $p_z$ . Therefore, only the lowest Landau level gives a nonvanishing contribution to the current, and we get from the surface contribution [19]

$$j_3 = N_c \sum_{f=u,d} \frac{q_f^2 \mu_5 B}{2\pi^2} = \frac{5\mu_5 e^2 B}{6\pi^2}, \quad (21)$$

which is certainly ultraviolet finite as it should be. Generally speaking, we should utilize a gauge-invariant regularization. Nevertheless, the above (21) indicates that a naive momentum cutoff can reproduce a correct expression for the anomalous chiral magnetic current.

The current density as given by Eq. (21) does not depend on quark mass explicitly or on temperature either. The reason is that the current is generated by the axial anomaly and it receives contributions only from the ultraviolet momentum regions (as the above derivation shows), and so it is insensitive to any infrared energy scales. Also, the Polyakov loop does not appear explicitly in Eq. (21). This is easy to understand; the Polyakov loop is a thermal coupling between quark excitations and the gluonic medium, and thus the Polyakov loop only enters the thermal part of  $\Omega$ . Since the current originates from the anomaly, however, the thermal part of  $\Omega$  just drops off for the current generation. The effect of the Polyakov loop will appear implicitly through the relation between  $\mu_5$  to  $n_5$ .

To confirm that our numerical prescription works well, we have computed  $j_3$  by means of Eq. (18) with  $\Omega$  given in Eq. (10). In Fig. 6, we show the results from our numerical computation as a function of  $\mu_5$ . In the figure we have plotted the normalized current

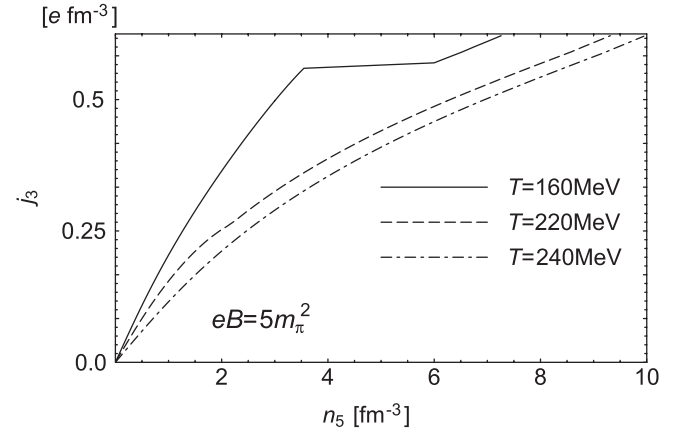
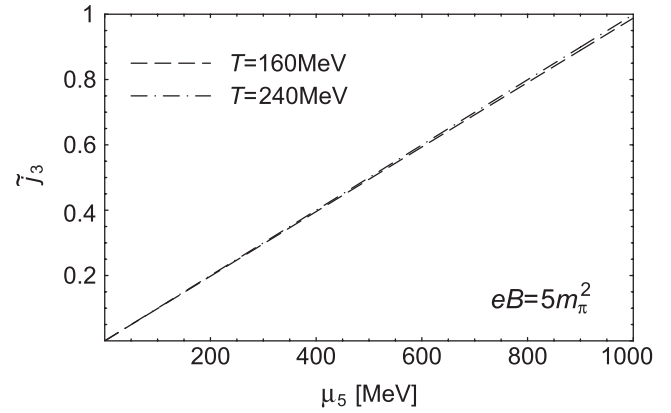


FIG. 6. (Upper panel) Normalized current density  $\tilde{j}_3 = (5\mu_0 e^2 B / 6\pi^2)^{-1} j_3$ , with  $\mu_0 = 1$  GeV, as a function of  $\mu_5$  at two different temperatures (below and above  $T_c$ ). (Lower panel) Current density as a function of  $n_5$  for  $eB = 5m_\pi^2$  computed at three different temperatures.

$$\tilde{j}_3 = \left( \frac{5\mu_0 e^2 B}{6\pi^2} \right)^{-1} j_3, \quad (22)$$

with a choice of  $\mu_0 = 1$  GeV, which we defined so as to make the comparison transparent at a glance. In Fig. 6, the dashed line represents  $\tilde{j}_3$  at  $T = 160$  MeV; on the other hand, the dotted-dashed line represents the case at  $T = 240$  MeV. We notice that our numerical results are perfectly in agreement with Eq. (21). We conclude that our numerical procedure correctly reproduces the expected dependence of  $j_3$  on  $\mu_5$  with the correct coefficient insensitive to infrared scales regardless of whether  $T$  is below or above  $T_c$ .

The result shown in the upper panel of Fig. 6 gives us confidence in our numerical procedure, but the figure itself is not yet more informative than Eq. (21). We express now  $j_3$  as a function of  $n_5$  using Eq. (21) and the results discussed in the previous section. The result of this computation is shown in the lower panel of Fig. 6, in which we plot the (not normalized) current density (measured in  $\text{fm}^{-3}$ ) as a function of  $n_5$  (measured in  $\text{fm}^{-3}$ ), at  $eB = 5m_\pi^2$  and at three different temperatures.

From Fig. 6 we notice that, at a fixed value of  $n_5$ , the larger the temperature is, the smaller  $j_3$  becomes. This seemingly counterintuitive result is easy to understand. As a matter of fact, as the temperature gets larger, the corresponding  $\mu_5$  for a given  $n_5$  should decrease because of more abundant thermal particles at higher temperature. Since  $j_3$  depends solely on  $\mu_5$ , a higher temperature requires a larger  $n_5$  to give the same  $j_3$ .

Besides  $j_3$ , another interesting quantity is the current susceptibility defined by

$$\chi_J = \langle j_3^2 \rangle - \langle j_3 \rangle^2 = - \left. \frac{1}{\beta V} \frac{\partial^2 \Omega}{\partial A_3^2} \right|_{A_3=0}. \quad (23)$$

If we naively use the above definition (23) for the cutoff model like the PNJL model,  $\chi_J$  is nonzero proportional to  $\Lambda^2$  even at  $T = B = 0$  as discussed in Ref. [27]. This is in contradiction with the gauge invariance, which requires the above susceptibility to vanish because the current susceptibility is nothing but the 33-component of the photon polarization tensor at zero momentum. Therefore, in order to deal with the physically meaningful quantity, we subtract the vacuum part from the above equation and compute

$$\bar{\chi}_J = \chi_J(\mu_5, B, T) - \chi_J(\mu_5, 0, 0) \quad (24)$$

to fulfill the requirement that photons are unscreened at  $T = B = 0$  regardless of any value of  $\mu_5$ .

We plot our results for  $\beta V \bar{\chi}_J$  as a function of  $eB$  in Fig. 7 at  $\mu_5 = 0$  (upper panel),  $\mu_5 = 200$  MeV (middle panel), and  $\mu_5 = 400$  MeV (lower panel). The oscillations in the susceptibility behavior are an artifact of the momentum cutoff. In these plots  $T_c = 228$  MeV denotes the critical temperature for chiral symmetry restoration at  $\mu_5 = B = 0$ .

Let us first focus on the case at  $\mu_5 = 0$ . At  $T = 0$  and  $T = 0.95T_c$ , the system is in the broken phase with  $\langle \bar{u}u \rangle \neq 0$  over the whole range of  $eB$ . On the other hand, at the temperature  $T = 1.1T_c$ , the system is in the chiral symmetric phase for  $eB$  smaller than a critical value. There is a phase transition from the symmetric to the broken phase with increasing  $eB$ . This transition is driven by the presence of the magnetic field as the catalysis of chiral symmetry breaking, as mentioned before. The effect of the phase transition leads to a cusp in the susceptibility  $\chi_J$  as a function of  $eB$ . We also notice that there seems to exist a range in  $eB$  in which  $\bar{\chi}_J < 0$ . This is a mere artifact of the momentum cutoff, which causes unphysical fluctuations in  $\bar{\chi}_J$ . The qualitative picture is similar also at  $\mu_5 \neq 0$ .

To distinguish physically meaningful information from cutoff artifacts, we have computed  $\chi_J$  by using a smoother regulator with  $N = 5$  in Eq. (12). We have readjusted the NJL parameters to keep the physical quantities ( $f_\pi$  and  $\langle \bar{u}u \rangle$ ) unchanged. Figure 8 is the result in which oscillations are suppressed and  $\chi_J > 0$  for any  $T$  and  $B$ .

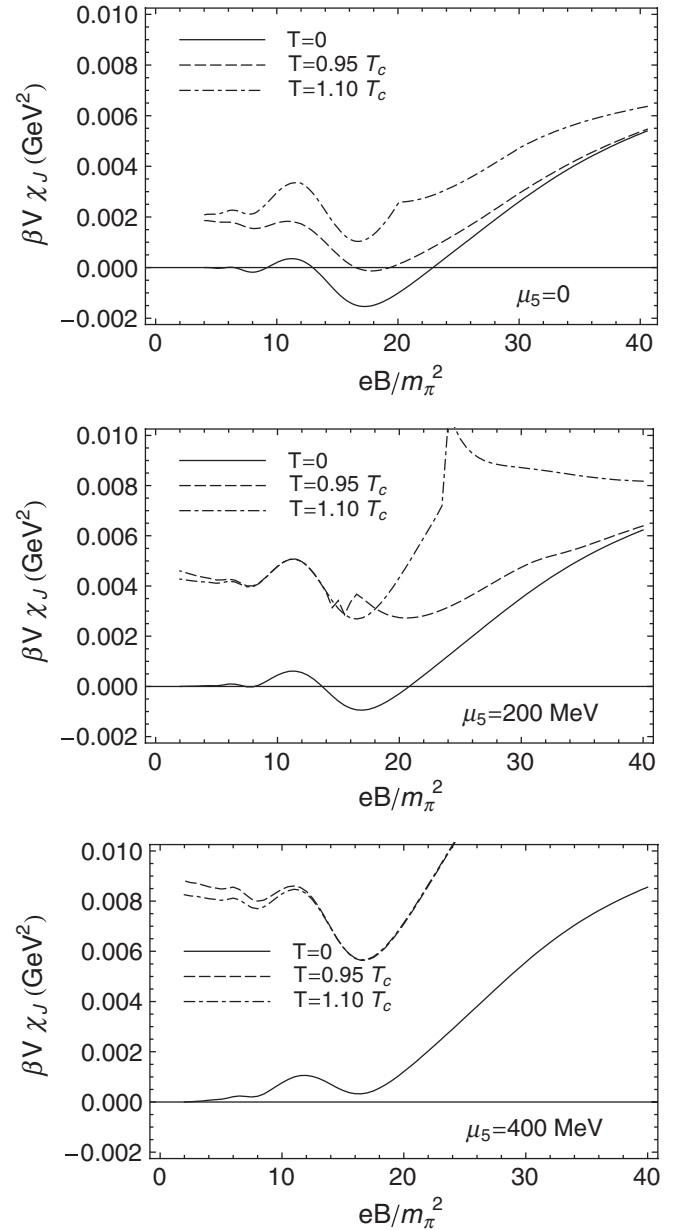


FIG. 7. Subtracted current susceptibility  $\beta V \bar{\chi}_J$  as a function of  $eB$  (in units of  $m_\pi^2$ ) for several different values of  $T$  (in units of  $T_c = 228$  MeV) and  $\mu_5$  (measured in MeV).

In view of Figs. 7 and 8, we can conclude that it is certainly a physical effect that the chiral phase transition critically affects the susceptibility  $\chi_J$  as well as  $\chi_5$ . As shown in Ref. [27], the susceptibility difference between the longitudinal and transverse directions has an origin in the axial anomaly and is insensitive to the infrared information. Nevertheless,  $\chi_J$  (and transverse  $\chi_J^T$ , too) should be largely enhanced near the chiral phase transition through mixing with the divergent chiral susceptibility, which is not constrained by anomaly. Such enhancement in  $\chi_J$  would ease the confirmation of the CME signals at experiment.

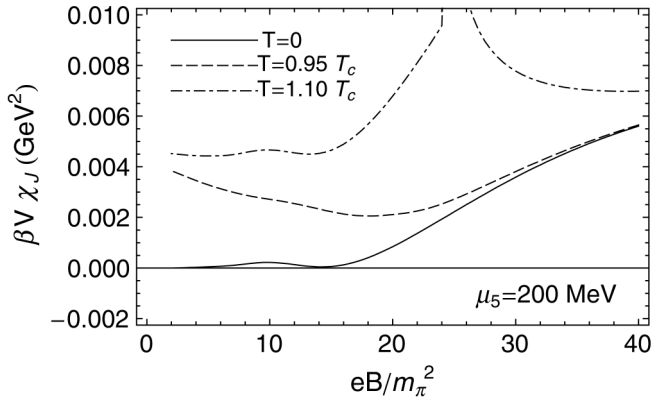


FIG. 8. Subtracted current susceptibility with a smoother regulator with  $N = 5$  in Eq. (12).

## V. CONCLUSIONS

In this paper, we have considered several aspects related to the response of quark matter to an external magnetic field. Quark matter has been modeled by the PNJL model, in which the QCD interaction among quarks is replaced by effective four-fermion interactions. In the PNJL model, besides the quark-antiquark condensate, which is responsible for the dynamical chiral symmetry breaking in the QCD vacuum, it is possible to compute the expectation value of the Polyakov loop, which is a relevant indicator for the quark deconfinement crossover.

In our study, we have first focused on the effect of a strong magnetic field on chiral symmetry restoration at finite temperature. Our results show the effect of the external field as a catalyzer of dynamical symmetry breaking. Moreover, the critical temperature increases as the strength

of  $B$  is increased. This behavior is in agreement with the previous studies on magnetic catalysis in NJL-like models.

We have also discussed the effects of a chiral chemical potential  $\mu_5$  on the phase structure of the model. The chiral chemical potential mimics the chirality induced by topological excitations according to the QCD anomaly relation. Instead of working at fixed chirality  $N_5$ , we have worked in the grand-canonical ensemble introducing  $\mu_5$ , i.e., the chemical potential conjugate to  $N_5$ . Besides the phase diagram of the model, summarized in Fig. 3, we have computed several quantities that are relevant for the CME. That is, we have computed the current density  $j_3$  and its susceptibility  $\chi_J$  as well as the chiral charge density  $n_5$  and its susceptibility  $\chi_5$ .

As a future project it is indispensable to extend our analysis to the  $2 + 1$  flavors and tune the PNJL-model parameters to reproduce the correct  $T_c$  and thermodynamic properties, which would enable us to make a serious comparison with the dynamical lattice-QCD data [29], and, furthermore, it would be possible to give a more pertinent prediction on the physical observables.

## ACKNOWLEDGMENTS

M.R. acknowledges discussions with H. Abuki and S. Nicotri, and K.F. thanks E. Fraga for discussions. The work of M.R. is supported by JSPS under Contract No. P09028. K.F. is supported by Japanese MEXT Grant No. 20740134 and also supported in part by Yukawa International Program for Quark Hadron Sciences. The numerical calculations were carried out on Altix3700 BX2 at YITP in Kyoto University.

- 
- [1] P. de Forcrand and O. Philipsen, *J. High Energy Phys.* **01** (2007) 077; **11** (2008) 012; Proc. Sci., LATTICE2008 (2008) 208.
- [2] Y. Aoki, Z. Fodor, S. D. Katz, and K. K. Szabo, *Phys. Lett. B* **643**, 46 (2006); Y. Aoki, S. Borsanyi, S. Durr, Z. Fodor, S. D. Katz, S. Krieg, and K. K. Szabo, *J. High Energy Phys.* **06** (2009) 088.
- [3] A. Bazavov *et al.*, *Phys. Rev. D* **80**, 014504 (2009).
- [4] M. Cheng *et al.*, [arXiv:0911.3450](https://arxiv.org/abs/0911.3450).
- [5] S. Muroya, A. Nakamura, C. Nonaka, and T. Takaishi, *Prog. Theor. Phys.* **110**, 615 (2003); K. Splittorff, Proc. Sci., LAT2006 (2006) 023 [[arXiv:hep-lat/0610072](https://arxiv.org/abs/hep-lat/0610072)]; K. Splittorff and J. J. M. Verbaarschot, *Phys. Rev. Lett.* **98**, 031601 (2007); K. Fukushima and Y. Hidaka, *Phys. Rev. D* **75**, 036002 (2007); J. C. R. Bloch and T. Wettig, *J. High Energy Phys.* **03** (2009) 100.
- [6] Z. Fodor and S. D. Katz, *J. High Energy Phys.* **03** (2002) 014.
- [7] C. R. Allton *et al.*, *Phys. Rev. D* **71**, 054508 (2005); R. V. Gavai and S. Gupta, *Phys. Rev. D* **78**, 114503 (2008).
- [8] J. Ambjorn, K. N. Anagnostopoulos, J. Nishimura, and J. J. M. Verbaarschot, *J. High Energy Phys.* **10** (2002) 062; Z. Fodor, S. D. Katz, and C. Schmidt, *J. High Energy Phys.* **03** (2007) 121.
- [9] M. D'Elia and M. P. Lombardo, *Phys. Rev. D* **67**, 014505 (2003); **70**, 074509 (2004); M. D'Elia, F. Di Renzo, and M. P. Lombardo, *Phys. Rev. D* **76**, 114509 (2007); P. de Forcrand and O. Philipsen, *Nucl. Phys.* **B673**, 170 (2003).
- [10] G. Aarts, *Phys. Rev. Lett.* **102**, 131601 (2009).
- [11] D. E. Kharzeev, L. D. McLerran, and H. J. Warringa, *Nucl. Phys.* **A803**, 227 (2008).
- [12] V. Skokov, A. Y. Illarionov, and V. Toneev, *Int. J. Mod. Phys. A* **24**, 5925 (2009).
- [13] S. P. Klevansky and R. H. Lemmer, *Phys. Rev. D* **39**, 3478 (1989); H. Suganuma and T. Tatsumi, *Ann. Phys. (N.Y.)* **208**, 470 (1991); I. A. Shushpanov and A. V. Smilga, *Phys. Lett. B* **402**, 351 (1997); D. N. Kabat, K. M. Lee, and E. J. Weinberg, *Phys. Rev. D* **66**, 014004 (2002); T. Inagaki, D.

- Kimura, and T. Murata, *Prog. Theor. Phys.* **111**, 371 (2004); T.D. Cohen, D.A. McGady, and E.S. Werbos, *Phys. Rev. C* **76**, 055201 (2007); K. Fukushima and H.J. Warringa, *Phys. Rev. Lett.* **100**, 032007 (2008); J.L. Noronha and I.A. Shovkovy, *Phys. Rev. D* **76**, 105030 (2007).
- [14] V.P. Gusynin, V.A. Miransky, and I.A. Shovkovy, *Nucl. Phys.* **B462**, 249 (1996); **B563**, 361 (1999); G.W. Semenoff, I.A. Shovkovy, and L.C.R. Wijewardhana, *Phys. Rev. D* **60**, 105024 (1999); V.A. Miransky and I.A. Shovkovy, *Phys. Rev. D* **66**, 045006 (2002).
- [15] E.S. Fraga and A.J. Mizher, *Phys. Rev. D* **78**, 025016 (2008); *Nucl. Phys.* **A831**, 91 (2009); J.K. Boomsma and D. Boer, [arXiv:0911.2164](https://arxiv.org/abs/0911.2164).
- [16] K.G. Klimenko, *Teor. Mat. Fiz.* **89**, 211 (1991) [*Theor. Math. Phys.* **89**, 1161 (1992)]; *Z. Phys. C* **54**, 323 (1992); *Teor. Mat. Fiz.* **90**, 3 (1992) [*Theor. Math. Phys.* **90**, 1 (1992)].
- [17] A.V. Zayakin, *J. High Energy Phys.* **07** (2008) 116; G. Lifschytz and M. Lippert, *Phys. Rev. D* **80**, 066005 (2009); **80**, 066007 (2009); H.U. Yee, *J. High Energy Phys.* **11** (2009) 085; B. Sahoo and H.U. Yee, [arXiv:0910.5915](https://arxiv.org/abs/0910.5915); A. Rebhan, A. Schmitt, and S.A. Stricker, [arXiv:0909.4782](https://arxiv.org/abs/0909.4782); S.I. Cui, Y.h. Gao, Y. Seo, S.j. Sin, and W.s. Xu, [arXiv:0910.2661](https://arxiv.org/abs/0910.2661); E. D'Hoker and P. Kraus, [arXiv:0911.4518](https://arxiv.org/abs/0911.4518).
- [18] E.V. Gorbar, S. Homayouni, and V.A. Miransky, *Phys. Rev. D* **72**, 065014 (2005).
- [19] K. Fukushima, D.E. Kharzeev, and H.J. Warringa, *Phys. Rev. D* **78**, 074033 (2008).
- [20] P. Arnold and L.D. McLerran, *Phys. Rev. D* **37**, 1020 (1988).
- [21] G.D. Moore, *Phys. Lett. B* **412**, 359 (1997); [arXiv:hep-ph/0009161](https://arxiv.org/abs/hep-ph/0009161); D. Bodeker, G.D. Moore, and K. Rummukainen, *Phys. Rev. D* **61**, 056003 (2000).
- [22] L.D. McLerran, E. Mottola, and M.E. Shaposhnikov, *Phys. Rev. D* **43**, 2027 (1991).
- [23] S.A. Voloshin, *Phys. Rev. C* **70**, 057901 (2004).
- [24] B.I. Abelev *et al.* (STAR Collaboration), [arXiv:0909.1717](https://arxiv.org/abs/0909.1717); *Phys. Rev. Lett.* **103**, 251601 (2009).
- [25] S.i. Nam, *Phys. Rev. D* **80**, 114025 (2009).
- [26] D.E. Kharzeev and H.J. Warringa, *Phys. Rev. D* **80**, 034028 (2009).
- [27] K. Fukushima, D.E. Kharzeev, and H.J. Warringa, [arXiv:0912.2961](https://arxiv.org/abs/0912.2961).
- [28] P.V. Buividovich, M.N. Chernodub, E.V. Luschevskaya, and M.I. Polikarpov, *Phys. Rev. D* **80**, 054503 (2009).
- [29] M. Abramczyk, T. Blum, G. Petropoulos, and R. Zhou, [arXiv:0911.1348](https://arxiv.org/abs/0911.1348).
- [30] P.N. Meisinger and M.C. Ogilvie, *Phys. Lett. B* **379**, 163 (1996).
- [31] K. Fukushima, *Phys. Lett. B* **591**, 277 (2004).
- [32] U. Vogl and W. Weise, *Prog. Part. Nucl. Phys.* **27**, 195 (1991); S.P. Klevansky, *Rev. Mod. Phys.* **64**, 649 (1992); T. Hatsuda and T. Kunihiro, *Phys. Rep.* **247**, 221 (1994); M. Buballa, *Phys. Rep.* **407**, 205 (2005).
- [33] A.M. Polyakov, *Phys. Lett.* **72B**, 477 (1978); L. Susskind, *Phys. Rev. D* **20**, 2610 (1979); B. Svetitsky and L.G. Yaffe, *Nucl. Phys.* **B210**, 423 (1982); B. Svetitsky, *Phys. Rep.* **132**, 1 (1986).
- [34] C. Ratti, M.A. Thaler, and W. Weise, *Phys. Rev. D* **73**, 014019 (2006); E. Megias, E. Ruiz Arriola, and L.L. Salcedo, *Phys. Rev. D* **74**, 114014 (2006); *Eur. Phys. J. A* **31**, 553 (2007); S. Roessner, C. Ratti, and W. Weise, *Phys. Rev. D* **75**, 034007 (2007); C. Sasaki, B. Friman, and K. Redlich, *Phys. Rev. D* **75**, 074013 (2007); S.K. Ghosh, T.K. Mukherjee, M.G. Mustafa, and R. Ray, *Phys. Rev. D* **77**, 094024 (2008); W.j. Fu, Z. Zhang, and Y.x. Liu, *Phys. Rev. D* **77**, 014006 (2008); M. Ciminale, R. Gatto, N.D. Ippolito, G. Nardulli, and M. Ruggieri, *Phys. Rev. D* **77**, 054023 (2008); Y. Sakai, K. Kashiwa, H. Kouno, and M. Yahiro, *Phys. Rev. D* **77**, 051901 (2008); **78**, 036001 (2008); K. Kashiwa, H. Kouno, and M. Yahiro, [arXiv:0908.1213](https://arxiv.org/abs/0908.1213); K. Fukushima, *Phys. Rev. D* **77**, 114028 (2008); **78**, 039902 (2008); H. Abuki, R. Anglani, R. Gatto, G. Nardulli, and M. Ruggieri, *Phys. Rev. D* **78**, 034034 (2008); H. Abuki, M. Ciminale, R. Gatto, and M. Ruggieri, *Phys. Rev. D* **79**, 034021 (2009); T. Hell, S. Roessner, M. Cristoforetti, and W. Weise, *Phys. Rev. D* **79**, 014022 (2009); [arXiv:0911.3510](https://arxiv.org/abs/0911.3510).
- [35] B.J. Schaefer, J.M. Pawłowski, and J. Wambach, *Phys. Rev. D* **76**, 074023 (2007).
- [36] J. Braun, L.M. Haas, F. Marhauser, and J.M. Pawłowski, [arXiv:0908.0008](https://arxiv.org/abs/0908.0008).
- [37] N.O. Agasian and S.M. Fedorov, *Phys. Lett. B* **663**, 445 (2008).
- [38] K. Fukushima, D.E. Kharzeev, and H.J. Warringa, [arXiv:1002.2495](https://arxiv.org/abs/1002.2495).
- [39] J. Wambach, B.J. Schaefer, and M. Wagner, [arXiv:0911.0296](https://arxiv.org/abs/0911.0296).
- [40] V.I. Ritus, *Ann. Phys. (N.Y.)* **69**, 555 (1972); *Zh. Eksp. Teor. Fiz.* **75**, 1560 (1978) [*Sov. Phys. JETP* **48**, 788 (1978)].
- [41] L. Campanelli and M. Ruggieri, *Phys. Rev. D* **80**, 034014 (2009).